

Crystallization of Pearl Biomineralization Protein in Microgravity Environments

Setsu NAKAE¹, Masafumi SHIONYU¹, Tomohisa OGAWA² and Tsuyoshi SHIRAI¹

Abstract

The isoforms of jacalin-related lectins of *Pteria penguin* PPL3 are known to regulate biomineralization of pearl shell, although the molecular mechanisms are largely unknown. The PPL3 crystal structures were determined partly by utilizing microgravity environments on the International Space Station for three isoforms, namely, PPL3A, PPL3B, and PPL3C. The crystals grown in microgravity environments tended to diffract to higher resolutions. The crystal structures revealed the structure stabilization mechanism of PPL3 isoforms through disulfide bond formations. Also the crystal structures, in combination with docking simulations to calcite, suggested a regulatory mechanism of biomineralization by carbohydrate-binding to the PPL3 isoforms. Additionally, the N-terminal residues of PPL3 isoforms were found in pyroglutamate form in the high-resolution electron densities, which was partly explained by the post-translational modification implied from the discrepancy between amino acid and gene sequences of PPL3 isoforms.

Keyword(s): Protein, Lectin; Biomineralization, Post-translational modification
Received 22 October 2018, Accepted 8 January 2019, Published 31 January 2019.

1. Introduction

Biomineralization is a process of selective extraction of metal ions into functional structures during the development of hard body parts of the organisms¹⁻⁴. The biominerals play important roles as the templates or nucleation centers for organic matrices. The knowledge of molecular mechanisms underlying the biomineralization process should be useful in various biomimetic nanotechnology applications

Calcium salts, namely, calcite, aragonite, and vaterite, are widely used in biomineralization by various organisms, including pearl shells⁵. Mother of pearl (nacre) is an organic-inorganic hybrid photonic crystal composed of aragonite tablets arranged in consecutive mineral lamellae, which generates structural colors of pearls. Another calcium salt, calcite, is also known as a major component of shells. The fluid secreted from the outer mantle epithelium of pearl shells contains various nacre matrix components, including the mineral precursors, polysaccharides, and a variety of proteins, which are thought to be required for the biomineralization process⁶. Although the molecular mechanisms underlying the biomineralization process has been expected to provide useful information for industries⁷, they are still largely unknown.

A series of lectins (carbohydrate-binding proteins) named PPLs (*Pteria penguin* lectins) have been recently identified in large-winged pearl shells. They have been demonstrated to affect pearl shell development in diverse manners⁸⁻¹⁰. These PPLs, namely, PPL2A, PPL2B, PPL3A, PPL3B, PPL3C, and PPL4, have been categorized into jacalin-related lectin (JRL) family based on the sequence similarities to the jacalin lectins from plant seeds¹¹.

Some of the PPLs were shown to regulate the growth of calcite crystals. The *in vitro* crystallization experiments revealed that

PPL3 isoforms and PPL4 were localized at the surface of calcite crystals¹⁰. The calcite crystal sizes under the presence of PPL3 were significantly small, indicating it suppressed the growth of calcite crystals by binding to the crystal surface. The number of calcite crystals increased depending on the concentration of PPL3 isoforms. The knockdown of PPL2A or PPL4 expression caused defects in the larva development of pearl shell *in vivo*, although the knockdown of PPL3 isoforms had no apparent effect.

However, the current knowledge on the roles of these lectins in pearl shell biomineralization is insufficient, and no significant picture has been obtained for their molecular mechanisms yet. The crystal structures of PPL3 isoforms were therefore determined in order to elucidate the molecular basis of the biomineralization mechanisms involving lectins partly by utilizing microgravity environments on the International Space Station (ISS)¹².

2. Crystallization and Crystallographic Analysis of PPL3 Isoforms

2.1 Microgravity Crystallization

PPL3 isoforms are dimeric lectins, and PPL3A, PPL3B, and PPL3C are homodimers of PPL3 α subunits, heterodimers of PPL3 α and PPL3 β subunits, and homodimers of PPL3 β subunits, respectively¹⁰. PPL3 α and PPL3 β subunits differ in only two sites: position 39 is Val in PPL3 α and Leu in PPL3 β , and position 86 is Glu in PPL3 α and Val in PPL3 β (**Fig. 1**). The protein samples of PPL3A, PPL3B, and PPL3C were prepared from the secretory fluid of the mantle of *Pteria penguin* and used for crystallization¹⁰.

The series of the High Quality Protein Crystal Growth Experiment JAXA-PCG#2-5 (from October 21 to 29, 2016) and JAXA-PCG#2-6 (from April 21 to June 2, 2017) supported by the

1 Department of Bioscience, Nagahama Institute of Bio-Science and Technology, 1266 Tamura-Cho, Nagahama, Shiga 526-0829, Japan.

2 Department of Biomolecular Science, Graduate School of Life Sciences, Tohoku University, Sendai, Miyagi 980-8577, Japan.
(E-mail: tomohisa.ogawa.c3@tohoku.ac.jp, t_shirai@nagahama-i-bio.ac.jp)

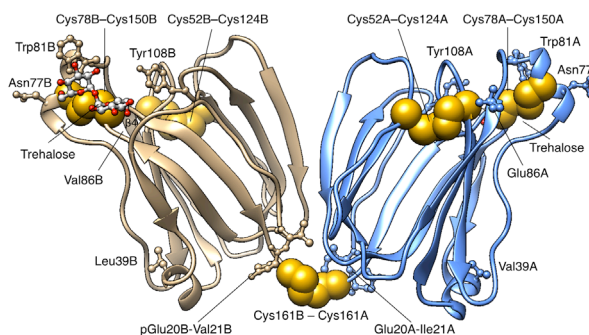


Fig. 1 The structure of PPL3B dimer is shown in ribbon model. The subunits A (PPL3 α) and B (PPL3 β) are colored light blue and light brown, respectively. The amino acid residues for disulfide bonds (Cys52-Cys124, Cys78-Cys150, and Cys161A-Cys161B) are shown in sphere-model (yellow). The residues different between PPL3 α and PPL3 β (Val/Leu39 and Glu/Val86), used for carbohydrate-binding (Asn77, Trp81, Glu86, and Tyr108), and modified post-translationally (Glu/pGlu20 and Ile/Val21) are shown in ball-and-stick models.

Japan Aerospace Exploration Agency (JAXA) were utilized for microgravity crystallization of the PPL3 isoforms^{13, 14}. The proteins were crystallized inside the Protein Crystallization Research Facility (PCRF) on board the pressurized module in the Japanese Experiment Module (JEM) Kibou on the ISS.

The microgravity crystallization experiments were executed by the counter diffusion method^{15, 16}. The 0.6–1.4% (*w/v*) protein solutions in 0.1 M ammonium sulfate and 12.5% (*w/v*) PEG 3350 solution in 25 mM Tris (for PPL3A isoform) or bis-Tris buffer (for PPL3B and C isoforms) at pH 5.5 were sealed in a capillary tube, where the protein solution was in contact with the crystallization buffer containing 0.2 M ammonium sulfate, 25% (*w/v*) PEG 3350, and the corresponding 0.1 M Tris or bis-Tris at pH 5.5. The protein solution and crystallization buffer were separated by a gel submerged with the crystallization buffer. For facilitate the crystallization, the solutions were seeded with crushed and diluted micro-crystals of the corresponding PPL3 isoform. The capillary tubes were packed in the JAXA Crystallization Box (JCB-SLG)^{17, 18}. The crystallization experiments were done at 293 K ambient temperature.

2.2 On Ground Crystallization

The PPL3 crystals were also grown on the ground by the hanging drop vapor diffusion method under the initial conditions using 0.2 M ammonium sulfate and 25% (*w/v*) PEG 3350 solution in 0.1 M Tris buffer at pH 5.5 for a 0.4 ml reservoir, and a mixture of 1 μ L of the reservoir solution and 1 μ L of 1% (*w/v*) protein solution for the hanging drop for PPL3A. PPL3C and PPL3B crystals were obtained in the solution of the same conditions of PPL3A, except that bis-Tris was used for the buffer reagent. The crystals grew in around one week to approximate maximum dimensions of 0.05 x 0.05 x 0.01 mm³ at 291 K ambient temperature.

2.3 X-ray Data Collection and Processing

A total of 18 (3), 13 (2), and 15(2) full sets of X-ray diffraction data were collected for PPL3A, PPL3B, and PPL3C, respectively (in parentheses are those of crystals grown in the microgravity environments). The diffraction experiments were executed by using the CCD detectors Rayonix/MX225HE, ADSC/ Q315, Rigaku/MSJ Jupiter-210, or DECTRIS/EIGER4M at the beam lines BL26B1, BL38B1, or BL41XU of SPring-8 (Hyogo, Japan). For cryoprotection, the crystals were soaked in an artificial mother liquor containing 15% (*v/v*) 2-methyl-2,4-pentanediol (MPD) for 10–30 s. To obtain the carbohydrate-bound structure of the PPL3 isoforms, specific carbohydrate (trehalose or isomaltose) was introduced into the crystals by soaking.

The diffraction images were processed by using the MOSFLM program¹⁹. The crystal structure of PPL3C was solved with the single isomorphous replacement by the anomalous-scattering (SIRAS) method using an Os-derivative crystal. The structures of other isoforms were determined by the molecular replacement method using the PPL3C crystal structure as a search model.

3. Effect of Microgravity Environments on PPL3 Crystals

3.1 Overall Quality of X-ray Data

The quality of the crystals appeared to be higher for the microgravity-grown crystals, and diffraction data of the highest resolution were obtained from the microgravity-grown crystals of PPL3A (1.4 Å resolution) and PPL3B (1.2 Å resolution) except for PPL3C¹². The averages of highest-resolutions and R_{sym} were better for the microgravity-grown crystals in comparison with the ground-grown ones (**Fig. 2**).

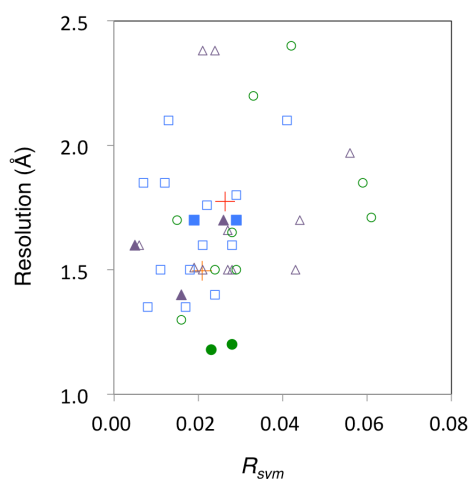


Fig. 2 The highest-resolution and R_{sym} values of the X-ray data presented in the original report, are plotted for PPL3A (purple triangles), PPL3B (green circles), and PPL3C (blue squares). The microgravity- and ground-grown crystals are indicated with filled and open markers, respectively. The orange and red crosses indicate the average values for microgravity- and ground-grown crystals, respectively.

Notably, the PPL3 isoforms were crystallized into two related orthorhombic $P2_12_12_1$ crystal form 1 (a, b, c) = (45, 50, 107) Å and form 2 (a, b, c) = (40, 73, 91) Å, and the asymmetric units contain one dimer in both crystal forms. PPL3A and PPL3C were exclusively crystallized into forms 1 and 2, respectively, and PPL3B was found in both forms. This is reasonable considering that the residues different between PPL3 α and PPL3 β subunits are involved in the crystal contacts. The microgravity-grown crystal data of PPL3B were obtained for form 1 crystals only. Thus, it was assumed that the effect of microgravity environments was rather significant for the form 1 crystals, from which the highest-resolution data for PPL3A and PPL3B were obtained.

3.2 Quantitative Comparisons of X-ray Data

The results implied that the microgravity-grown crystals of PPL3 isoforms have a potential for atomic resolution structure analyses. However, the X-ray data collection conditions, for example, detectors, exposure time, or oscillation angle, were not coordinated among the crystals, and subjective comparisons were not done in the original report¹².

Therefore, the diffraction images were re-processed in same resolution range from 20.0 to 1.7 Å for the crystals, which diffracted higher than 1.7 Å resolution, for 11 (3), 9 (2), 9 (2) crystals of PPL3A, PPL3B, and PPL3C, respectively (in parentheses are the number of microgravity-grown crystals) for a comparison purpose. The R_{sym} , R_{meas} , R_{pim} , mosaicity, $\langle I/\sigma \rangle$,

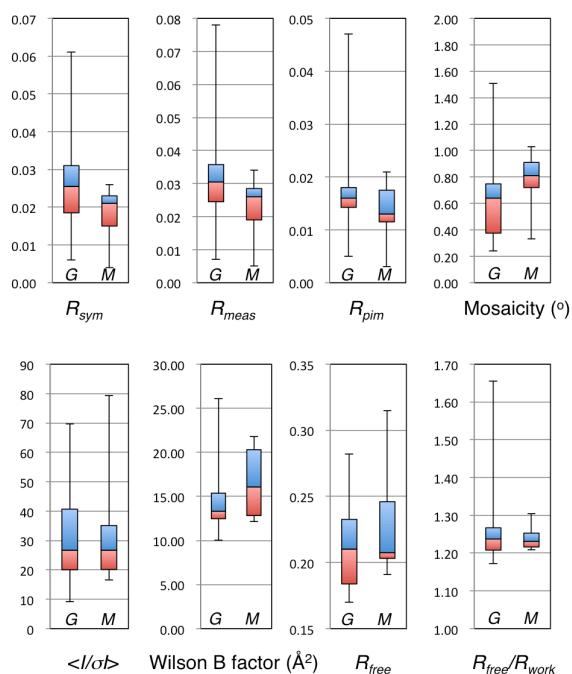


Fig. 3 The distributions of R_{sym} , R_{meas} , R_{pim} , mosaicity, $\langle I/\sigma \rangle$, Wilson B factor, R_{free} , R_{free}/R_{work} values for ground- (G) and microgravity-grown (M) crystals of PPL3 isoforms are shown in box-and-whisker plots

Wilson B factor, R_{free} , R_{free}/R_{work} values for ground- and microgravity-grown crystals are compared to each other. R_{work} and R_{free} values were those of the protein structure models, which were tentatively refined against the corresponding diffraction data (Fig. 3).

In this subjective and quantitative comparison, the R_{sym} , R_{meas} , and R_{pim} values tended to be better for the microgravity-grown crystals, although statistically significant difference was observed only for the R_{sym} values, showing $p = 0.045$ in t -test. The other parameters, namely, mosaicity, $\langle I/\sigma \rangle$, Wilson B factor, R_{free} , and R_{free}/R_{work} values, did not show significant difference between ground- and microgravity-grown crystals.

The effect of the microgravity environments appeared to be a modest improvement in diffraction spot quality, which was reflected to the R_{sym} values. The analyses should remain to be tentative, because the number of microgravity-grown crystals was still limited, and the crystallization conditions were differently tuned for the microgravity experiments from that of the on ground experiments, for example, the protein solutions were seeded in the microgravity experiments in order to ensure crystal growth during the flight time. It should be also noted that the difference in the crystallization methods between the microgravity (counter diffusion method) and the most of on ground (hanging drop vapor diffusion method) experiments was ignored in order to secure the sample number.

4. Knowledge from PPL3 Crystal structures

4.1 Structure-Stabilization by Disulfide Bonds

The high-resolution crystal structures revealed that the subunit structures were highly conserved among the isoforms (Fig. 1). As a remarkable structural feature, two disulfide bonds, Cys52-Cys124 and Cys78-Cys150, were formed within each subunit, and the latter one connected the $\alpha 2$ -helix to the other parts. The $\alpha 2$ -helix is used for carbohydrate binding. These intra-subunit disulfide bonds and the counter part of $\alpha 2$ -helix were found only in PPL3 isoforms and the closely related homologs (PPL2 isoforms and PPL4) at this point of time. Furthermore, the PPL3 subunits were covalently connected through an inter-subunit disulfide bond between C-termini (Cys160A-Cys160B), which was also found only in the closely related homologs of PPL3 isoforms.

Consequently, the complexes of PPL3 isoforms were quite stable during purification and crystallization, and the heterodimer, PPL3B, rarely rearranged into the homodimeric PPL3A or PPL3C, due to the inter-subunits disulfide bond. PPL3 showed full hemagglutination activity even after incubation at 60°C for 60 minutes¹⁰. Considering that PPL3 isoforms must function in the extracellular and high salt concentration environments, the observed structure stabilization should be required for the pearl shell lectins.

4.2 Provable Carbohydrate-Regulation of Biomineralization

In order to predict the calcite-interacting regions of PPL3 isoforms, computational docking simulations of the PPL3B crystal structure to the models of representative calcite crystal

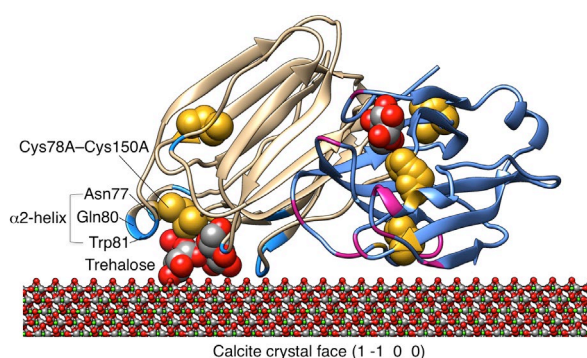


Fig. 4 Top-scored pose of PPL3B on calcite crystal face (1 - 1 0 0) is shown. The calcite atoms are shown in elementary coloring in the bottom. The PPL3B is shown in ribbon model as in Fig. 1, and the positions of the interface residues suggested by docking simulation are shown in magenta and blue for subunits A and B, respectively. The trehalose ligands are shown in elementary colored sphere model. The disulfide-bond Cys78-Cys150 and interface residues on α 2-helix are indicated.

faces were performed¹²⁾. Ten best solutions were selected for each crystal face, and the frequencies of the PPL3B residues used for calcite interactions were evaluated.

The results suggested that the residues on the carbohydrate-binding site, including Asn77, Gln80, and Trp81 on α 2-helix, might also take part in calcite-binding (Fig. 4). Interestingly, the peptide segment containing α 2-helix appeared to be disordered (demonstrating obscure electron density maps) in the crystals of carbohydrate-unbound PPL3 isoforms, and its conformation was stabilized when a specific carbohydrate (trehalose or isomaltose) was bound.

The observation suggested that the formation of calcite-binding structure required a binding of specific carbohydrates to PPL3 isoforms. It implied a regulatory role of the carbohydrates in calcite crystal growth through PPL3 isoforms, and provided the first clue for the molecular mechanisms of biomineralization by lectins.

4.3 Novel post-transcriptional modification

The high-resolution electron density obtained from the microgravity-grown crystals also provided an important clue for another mystifying character of the PPL3 isoforms. It has been previously found that the N-terminal peptides of the PPL3 isoforms were Gln20-Val21 according to the cDNA sequencing but Glu20-Ile21 from the peptide analyses by Edman degradation.

The PPL3 crystal structures revealed that the majority of the N terminus was in pGlu (pyroglutamate) form, and the 21st site was consistent with the genome sequence (Val21) when position 20 was pGlu (Fig. 5). pGlu is formed by both spontaneous and enzymatic cyclization of N-terminal glutamate (Glu) or glutamine (Gln) *in vivo*²⁰⁾. This explains why only the Glu20-Ile21 sequence was detected in the Edman degradation, because pGlu did not degrade in the reaction.

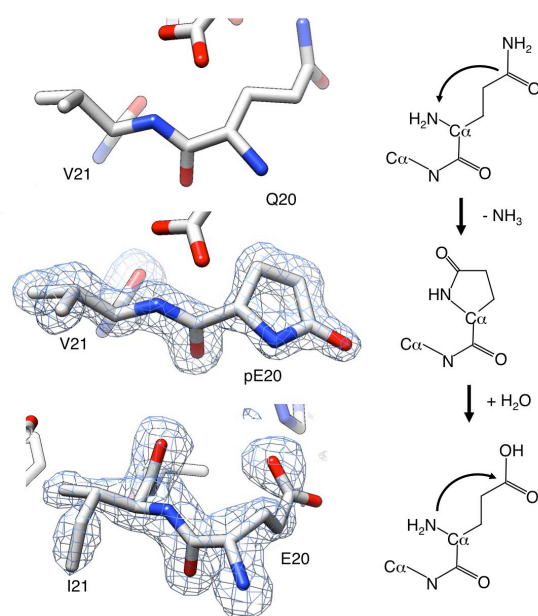


Fig. 5 The residues Gln20-Val21 (top) predicted from the gene sequence were not observed in the electron densities. The $F_o - F_c$ omit maps (electron densities) of pGlu(pyroglutamate)20-Val21 (middle) and Glu20-Ile21 (bottom) are superposed on the crystal structures. The omit maps are contoured at 2.5σ and 3.0σ for pGlu(pyroglutamate)20-Val21 and Glu20-Ile21, respectively.

It was also observed in the crystal structures that non-cyclized N-termini existed as a minor fraction, and the 21st site appeared to be Ile21, when the 20th site did not look like pGlu. Gln20 cyclized into pGlu20 can be converted into Glu20, which is consistent with the peptide analysis, in a decyclization reaction. It suggests that this possible post-transcriptional modification would be initiated by a cyclization of Gln20, and the conversion of Val21 to Ile21 is coupled, with a still unknown reaction, to decyclization of pGlu20 into Glu20.

These findings provided an important clue in elucidating this probably novel post-transcriptional modification of proteins. To further elucidate this process, determination of the structures of PPL3 isoforms in atomic resolution should be required.

5. Conclusion

The quality of the X-ray data from PPL3A, PPL3B, and PPL3C crystals were modestly improved by utilizing the microgravity environments in the ISS. The high-resolution electron densities contributed to reveal a novel post-translational modification and the first molecular basis of regulatory mechanisms of calcite crystal growth through carbohydrate binding to the biomineralization-related lectins.

Acknowledgments

We are grateful to the Japan Aerospace Exploration Agency (JAXA) for the support in the High-Quality Protein Crystal

Growth Experiment on JEM/ISS (JAXA PCG #2-5 & #2-6), the Japan Synchrotron Radiation Research Institute (JASRI) for the support at the synchrotron facilities at SPring-8 (proposal No. 2012B1254), the Ministry of Education, Science and Culture of Japan (MEXT) for the supports from Grants-in-aid for scientific research (JP17H01818 to T.S. and 25107703 and 23107505 to T.O.), and the Japan Agency for Medical Research and Development (AMED) for the support form Basis for Supporting Innovative Drug Discovery and Life Science Research (BINDS) (17am0101111j0001) to T.S.

References

- 1) L. Addadi and S. Weiner: *Angewandte Chem. Int. Edition in English*, **31** (1992) 153.
- 2) M.E. Marsh: *Comp. Biochem. Physiol. B. Biochem. Mol. Biol.*, **136** (2003) 743.
- 3) G. Mayer: *Science*, **310** (2005) 1144.
- 4) E. Bäuerlein: *Growth and Form, What is the Aim of Biomineralization? Handbook of Biomineralization*, Wiley-VCH Verlag GmbH2008, p. 1.
- 5) R. Brooks, L.M. Clark and E.F. Thurston: *Philos. Trans. Royal Soc. A, Mathematical and Physical Sciences*, **243** (1950) 145.
- 6) S. Weiner: *CRC Crit. Rev. Biochem.*, **20** (1986) 365.
- 7) C. Sanchez, H. Arribart and M.M. Guille: *Nat. Mater.*, **4** (2005) 277.
- 8) T. Naganuma, T. Ogawa, J. Hirabayashi, K. Kasai, H. Kamiya and K. Muramoto: *Mol. Divers*, **10** (2006) 607.
- 9) T. Naganuma, W. Hoshino, Y. Shikanai, R. Sato, K. Liu, S. Sato, K. Muramoto, M. Osada, K. Yoshimi, T. Ogawa: *PLoS One.*, **9** (2014) e112326.
- 10) T. Ogawa, R. Sato, T. Naganuma, K. Liu, T. Hashimoto, A.E. Lakudzala, M. Osada, K. Yoshimi, J. Hirabayashi, H. Tateno, K. Muramoto: to be published. (2018).
- 11) W.J. Peumans, E.J. Van Damme, A. Barre and P. Rouge: *Adv. Exp. Med. Biol.*, **491** (2001) 27.
- 12) S. Nakae, M. Shionyu, T. Ogawa and T. Shirai: *Proteins*, **86** (2018) 644.
- 13) S. Takahashi and H. Tanaka: *Int. J. Microgravity Sci. Appl.*, **34** (2017) 340103.
- 14) K. Inaka, S. Takahashi and H. Tanaka: *Int. J. Microgravity Sci. Appl.*, **34** (2017) 340104.
- 15) J.M. Garcia-Ruiz: *Methods Enzymol*, **368** (2003) 130.
- 16) F. Otalora, J.A. Gavira, J.D. Ng and J.M. Garcia-Ruiz: *Prog. Biophys. Mol. Biol.*, **101** (2009) 26.
- 17) H. Tanaka, K. Inaka, S. Sugiyama, S. Takahashi, S. Sano, M. Sato, S. Yoshitomi: *J. Synchrotron Radiat.*, **11** (2004) 45.
- 18) S. Takahashi, K. Ohta, N. Furubayashi, B. Yan, M. Koga, Y. Wada, M. Yamada, K. Inaka, H. Tanaka, H. Miyoshi, T. Kobayashi, S. Kamigaichi: *J. Synchrotron Radiat.*, **20** (2013) 968.
- 19) T.G. Battye, L. Kontogiannis, O. Johnson, H.R. Powell and A.G. Leslie: *Acta. Crystallogr D. Biol. Crystallogr.*, **67** (2011) 271.
- 20) R.W. Garden, T.P. Moroz, J.M. Gleeson, P.D. Floyd, L. Li, S.S. Rubakhin, J.V. Sweedler: *J. Neurochem.*, **72** (1999) 676.